# A Design of the Novel Coupled-Line Bandpass Filter Using Defected Ground Structure With Wide Stopband Performance

Jun-Seok Park, *Associate Member, IEEE*, Jun-Sik Yun, and Dal Ahn, *Member, IEEE*

***Abstract*—In this paper, a novel three-pole coupled-line bandpass filter with a microstrip configuration is presented. Presented bandpass filters use defected ground structure (DGS) sections to simultaneously realize a resonator and an inverter. The proposed coupled-line bandpass filter provides compact size with low insertion-loss characteristic. Furthermore, a DGS shape for a microstrip line is newly proposed. The proposed DGS unit structure has a resonance characteristic in some frequency band. The proposed coupled-line filter can provide attenuation poles for wide stopband characteristic due to resonance characteristic of DGS. The equivalent circuit for the proposed DGS unit section is described. The equivalent-circuit parameters for DGS are extracted by using a three-dimensional finite-element-method calculation and simple circuit analysis method. A design method for the proposed coupled-line filter is derived based on coupled-line filter theory and the equivalent circuit of the DGS. The experimental results show excellent agreements with theoretical simulation results.**

***Index Terms*—Attenuation pole, coupled-line bandpass filter, defected ground structure.**

## I. Introduction

RECENTLY, research on the defected ground structure (DGS) such as a photonic bandgap (PBG) transmission line, which has periodic arrays of defects, has been reported with various configurations in microwave and millimeter frequency-band applications. [1]–[3] The DGS with periodic or nonperiodic arrays provides a rejection band in some frequency range due to the increase of the effective inductance of a transmission line. [4], [5] This rejection characteristic of the DGS is available to many circuits such as a power-amplifier module, planar antennas, power dividers and filters, etc. [5]–[9] However, in order to apply pertinently peculiar characteristics of a DGS to a practical circuits, the modeling procedure for a DGS should be preceded. Various efforts on finding the equivalent circuit and parameters of a DGS are required.

In this paper, a new etched DGS shape for the implementation of coupled-line filter is proposed. An etched defect disturbs the shield current distribution in the ground plane. This disturbance can change characteristics of a transmission line such as line capacitance and inductance. The proposed DGS consists of narrow and wide etched areas in the backside metallic ground plane, which give rise to increasing the effective capacitance and inductance of a transmission line, respectively. Thus, an *LC* equivalent circuit can represent the proposed unit DGS circuit. [8], [9] Effects on these equivalent-circuit parameters due to a physical dimension variation of the proposed DGS are detailed more in [8] and [9]. In order to extract the equivalent-circuit parameters for the DGS section, $S$-parameters of the proposed DGS unit section were calculated by using a three-dimensional finite-element method (FEM) simulator. The method for finding the equivalent-circuit parameters is also detailed more in [8] and [9]. In this paper, a novel three-pole coupled-line bandpass filter with DGS sections, which is shown in Fig. 1, is proposed. The proposed coupled-line filter has a microstrip resonator and two DGS sections at the in–out port. DGS sections in the proposed coupled-line bandpass filter can be performed simultaneously as a resonator and inverter. Thus, a three-pole bandpass filter can be realized by the proposed filter configuration with only a single resonator. The proposed coupled-line bandpass filter provides more compact size and an excellent insertion-loss characteristic compared to a conventional coupled-line bandpass filter. In addition, the DGS has a self-resonant frequency. Due to this self-resonant characteristic of the DGS section, the proposed bandpass filter structure can provide an attenuation pole in the upper stopband. Due to this attenuation pole, the stopband is wider than that of conventional coupled-line filters. In order to derive an equivalent circuit for the proposed coupled-line bandpass filter, we employ equivalent circuit and extraction methods

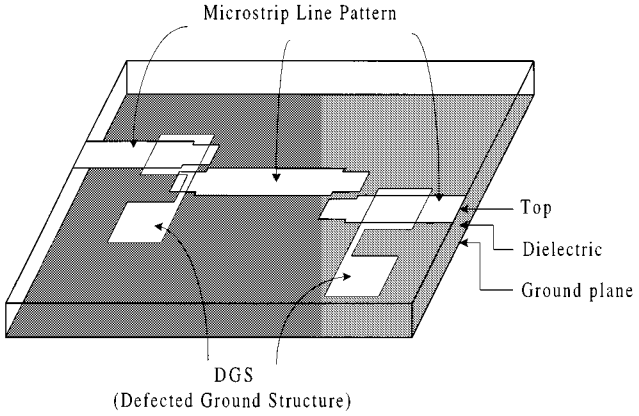


Fig. 1. Schematic of the proposed three-pole coupled-line bandpass filter with two DGS sections, which are located on the backside metallic ground plane.

Manuscript received December 29, 2000. This work was supported by the Korea Foundation under Grant KRF-2001-042-E00041.

J.-S. Park and D. Ahn are with the Division of Information Technology Engineering, Soonchunhyang University, Choongnam, Korea (e-mail: jspark@ramrec.sch.ac.kr).

J.-S. Yun was with the Division of Information Technology Engineering, Soonchunhyang University, Choongnam, Korea. He is now with Ansoft Corporations, Seoul, Korea.

Publisher Item Identifier 10.1109/TMTT.2002.802313.

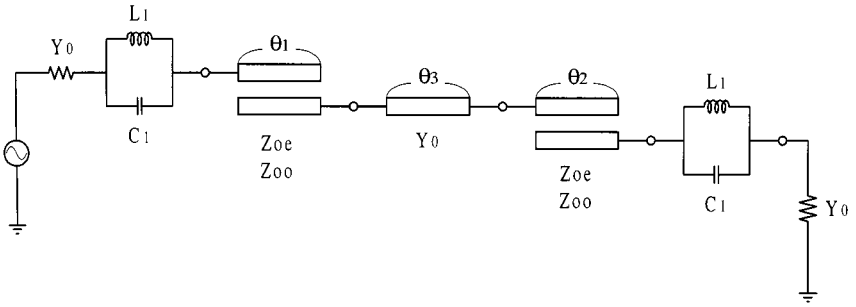


Fig. 2. Circuit representation of the three-pole coupled-line bandpass filters with equivalent circuits of the DGS, which are represented by a parallel *LC* circuit.

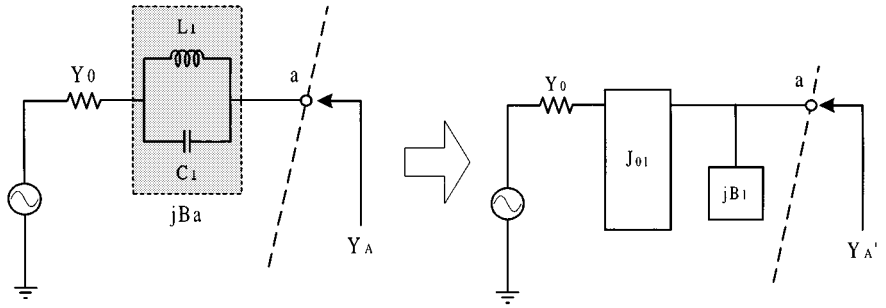


Fig. 3. Converting *LC* resonator circuit into a $J$-inverter and a parallel resonator.

of circuit parameters for a DGS, which are described in [8] and [9]. By replacing DGS sections with the derived equivalent circuits, the design formula for the proposed coupled-line bandpass filter can be derived based on the coupled-line filter theory. Moreover, the design method of a compact DGS coupled-line filter with multiple poles of attenuation at the upper stopband is derived to realize more improved stopband characteristic. This multiple poles can be implemented by putting another DGS in the resonator section. We implemented proposed three-pole coupled-line bandpass filters with a microstrip to show validity of proposed filter configurations and derived design methods. Measurements on the fabricated DGS coupled-line filters show excellent agreement with theoretical results.

## II. Design Theory

Fig. 1 shows the proposed coupled-line bandpass filter configuration with two DGS sections, which is located on the backside metallic ground plane. The DGS sections can be replaced with parallel *LC* resonators, as shown in Fig. 2. The series susceptance for a parallel *LC* resonator, shown in Fig. 2, which corresponds to the DGS section, can be converted to a parallel resonator with a $J$-inverter, as shown in Fig. 3. Thus, the proposed bandpass filter has a three-pole bandpass-filter characteristics. The relations between the two circuits shown in Fig. 3 can be derived from equality between $Y_a$ and $Y_a'$, as shown in Fig. 3, which are input admittances seen to source. The $J$-inverter formula and resonator susceptance are then given by

$$J_{01} = \sqrt{\frac{B_a^2}{1+\left(\frac{B_a}{Y_0}\right)^2}} \tag{1}$$

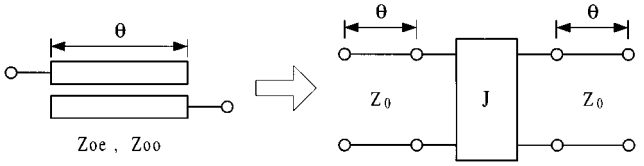


(a) (b)

Fig. 4. Equivalent circuit of a parallel coupled-line with two opened terminations. The equivalent circuit has a $J$-inverter with two transmission-line sections.

$$B_1 = \frac{B_a}{1+\left(\frac{B_a}{Y_0}\right)^2} \tag{2}$$

where $B_a = \omega_{c1}C_1(\omega/\omega_{c1} - \omega_{c1}/\omega)$, which is susceptance of the DGS section.

$B_1$ is the susceptance of the equivalent resonator for the DGS section. $\omega_{c1}$ then denotes the angular resonant frequency of the parallel *LC* resonator, shown in Fig. 2, and $C_1$ denotes the extracted capacitance value for a DGS. At this resonant frequency of the DGS circuit, the $J$-inverter value becomes zero. This means that there is no coupling at this frequency such as dc. Thus, the proposed bandpass-filter structure can provide an attenuation pole at the resonant frequency of the DGS circuit. In addition, the coupled-line section can be transformed to the $J$-inverter with transmission lines at both ends, as shown in Fig. 4. The equivalent relation between a coupled-line circuit and the $J$-inverter circuit with transmission lines is given as follows:

$$Z_{oe} = \frac{Z_o \sin\theta\left(\sin\theta + JZ_o + J^2 Z_o \sin\theta\right)}{\sin^2\theta - J^2 Z_o^2 \cos\theta} \tag{3}$$

$$Z_{oo} = \frac{Z_0 \sin\theta\left(\sin\theta - JZ_0 + J^2 Z_0 \sin\theta\right)}{\sin^2\theta - J^2 Z_0^2 \cos\theta}. \tag{4}$$

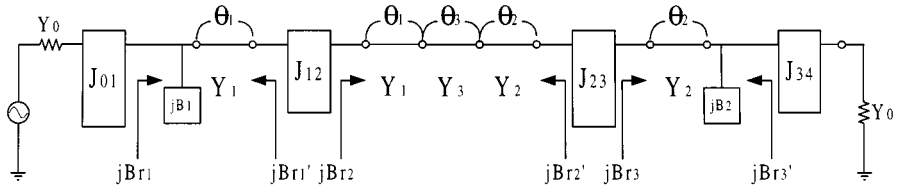


Fig. 5. Equivalent circuit of the proposed three-pole coupled-line bandpass filter with two DGS sections. $jB_{r1}$ denotes the susceptances of each resonators toward corresponding directions.

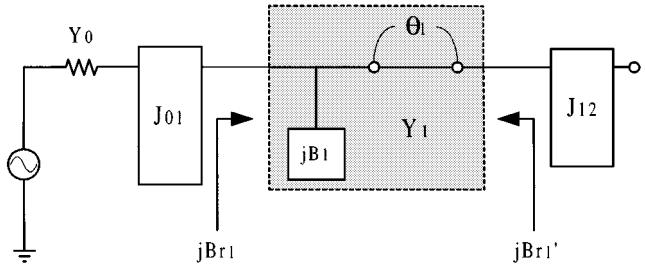


Fig. 6. Equivalent circuit of the first resonator section, which includes a part of the DGS equivalent circuit.

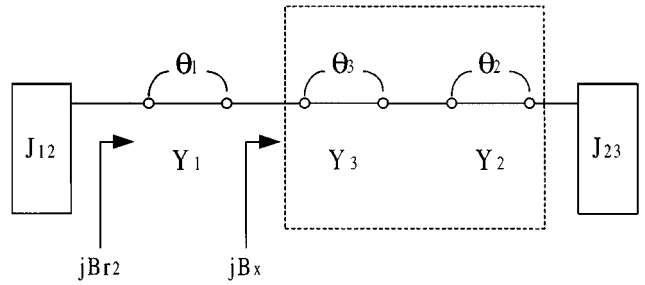


Fig. 7. Equivalent circuit of the second resonator section.

$Z_{oe}$ and $Z_{oo}$ in (3) and (4) denotes the even and odd impedance of the coupled-line circuit, respectively. By using equivalent circuits for DGS sections and coupled-line circuits, the equivalent circuit of the proposed coupled-line bandpass filter with a DGS can be expressed as shown in Fig. 5. In order to derive the design formula, which means the $J$-inverter formula, for the given specifications, the susceptances for each equivalent resonator shown in Figs. 6 and 7 should be derived. For the first resonator, susceptances for each direction are given as follows:

$$jB_{r1} = j\left(B_1 + Y_1 \tan\theta_1\right) \tag{5}$$

$$jB'_{r1} = jY_1 \tan\left(\theta_1 + \alpha\right) \tag{6}$$

where $\alpha = \tan^{-1}(B_1/Y_1)$.

For the second resonator, susceptances are given as follows:

$$jB_{r2} = jY_1 \tan\left(\theta_1 + \phi'\right) \tag{7}$$

$$jB'_{r2} = jY_2 \tan\left(\theta_2 + \phi''\right) \tag{8}$$

where $\phi' = \tan^{-1}((Y_3/Y_1)\tan(\theta_3 + \theta'))$, $\theta' = \tan^{-1}((Y_2/Y_3)\tan\theta_2)$, $\phi'' = \tan^{-1}((Y_3/Y_2)\tan(\theta_3 + \theta''))$, and $\theta'' = \tan^{-1}((Y_1/Y_3)\tan\theta_1)$.

Also, for the third resonator, susceptances are given as follows:

$$jB_{r3} = jY_2 \tan\left(\theta_2 + \beta\right) \tag{9}$$

$$jB'_{r3} = j\left(B_2 + Y_2 \tan\theta_2\right) \tag{10}$$

where $\beta = \tan^{-1}(B_2/Y_2)$, $B_2$ is the susceptance of the equivalent resonator for the second DGS section. In addition, by using resonance conditions of the first and second resonator, electrical lengths for each coupled section can be derived as follows:

$$\theta_1 = \tan^{-1}\left\{\frac{\omega_{c1}C_1 \cdot \left(\dfrac{\omega_{c1}}{\omega_0} - \dfrac{\omega_0}{\omega_{c1}}\right)}{Y_1\left(1 + \left(\dfrac{B_a}{Y_0}\right)^2\Big|_{\omega=\omega_0}\right)}\right\} \cdot \frac{\omega}{\omega_0} \tag{11}$$

$$\theta_2 = \tan^{-1}\left\{\frac{\omega_{c2}C_2 \cdot \left(\dfrac{\omega_{c2}}{\omega_0} - \dfrac{\omega_0}{\omega_{c2}}\right)}{Y_2\left(1 + \left(\dfrac{B_b}{Y_0}\right)^2\Big|_{\omega=\omega_0}\right)}\right\} \cdot \frac{\omega}{\omega_0} \tag{12}$$

where $B_b$ is the susceptance of the second DGS section. $\omega_{c2}$ denotes the angular resonant frequency of the parallel *LC* resonator and $C_2$ denotes the extracted capacitance value for the second DGS. As a result, the $J$-inverter formula is given as follows:

$$J_{01} = \sqrt{\frac{Y_0 B_{r1}(\omega_2)}{\omega'_1 g_0 g_1}} = \sqrt{\frac{(B_a)^2\Big|_{\omega=\omega_0}}{1 + \left(\dfrac{B_a}{Y_0}\right)^2\Big|_{\omega=\omega_0}}} \tag{13}$$

$$J_{12} = \sqrt{\frac{B'_{r1}(\omega_2)\, B_{r2}(\omega_2)}{\omega'_1 g_1 \omega'_1 g_2}} \tag{14}$$

$$J_{23} = \sqrt{\frac{B'_{r2}(\omega_2)\, B_{r3}(\omega_2)}{\omega'_1 g_2 \omega'_1 g_3}} \tag{15}$$

$$J_{34} = \sqrt{\frac{Y_0 B'_{r3}(\omega_2)}{\omega'_1 g_0 g_4}} = \sqrt{\frac{(B_b)^2\Big|_{\omega=\omega_0}}{1 + \left(\dfrac{B_b}{Y_0}\right)^2\Big|_{\omega=\omega_0}}}. \tag{16}$$

The derived design method for the proposed DGS coupled line can be directly adapted to design a practical filter. Furthermore, from derived design equations, it has been shown that the DGS section in the proposed coupled-line bandpass filter is operated simultaneously as a resonator and inverter. In the following section, we will demonstrate an example for bandpass filter design with the derived filter equivalent circuit and equations.

## III. Implementation and Experiments

To demonstrate the validity of the proposed coupled-line bandpass-filter structure and design method, we designed a

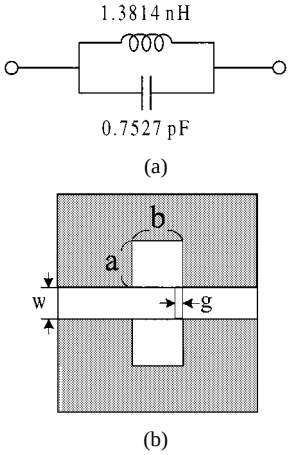


Fig. 8. (a) Equivalent-circuit parameters of the DGS section for realization of the designed coupled-line bandpass filter. (b) Corresponding DGS circuit to the determined parallel *LC* resonator. The gap distance $g$ is 0.3 mm. The lattice dimension is $a = 3.45$ mm and $b = 3.5$ mm. The conductor width $W$ is 1.5 mm.

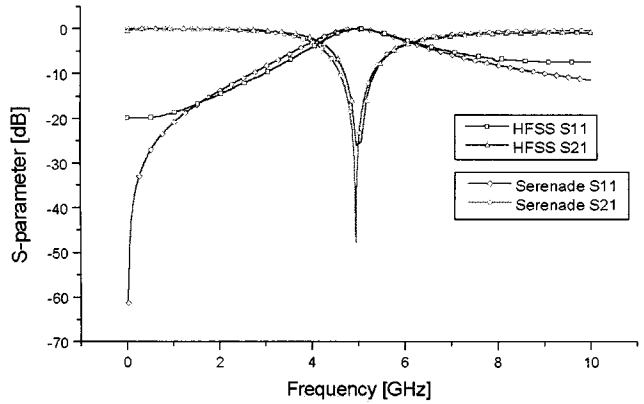


Fig. 9. Comparative results between the $S$-parameters of the circuit simulation and the 3-D FEM calculation for the designed DGS circuit.

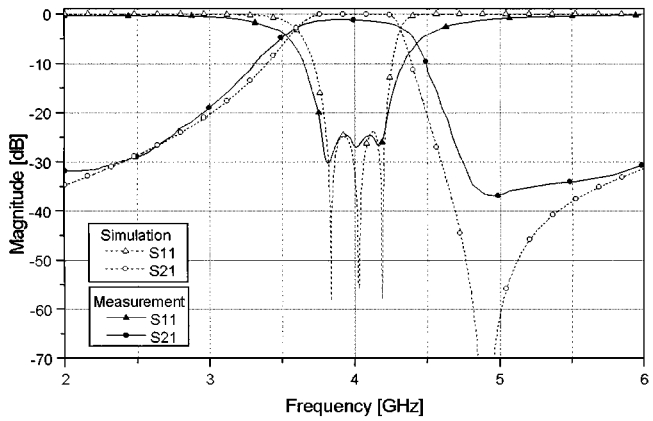


Fig. 10. Comparison between simulation and measurement on the fabricated DGS coupled-line bandpass filter.

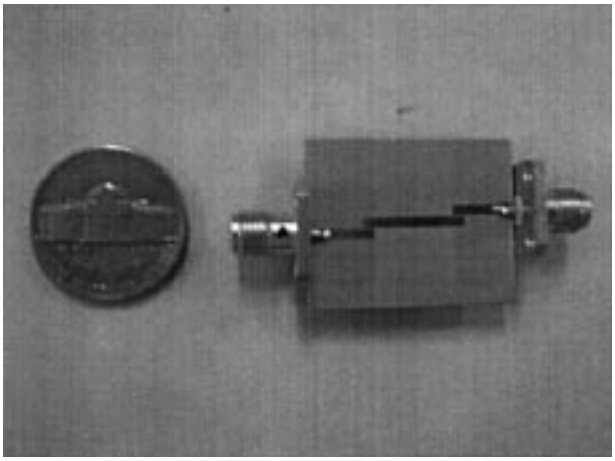

(a)

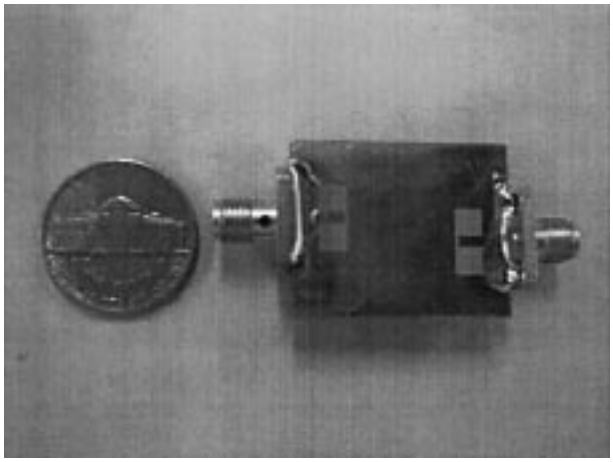

(b)

Fig. 11. Fabricated coupled-line bandpass filter with DGS. (a) Top view. (b) Bottom view.

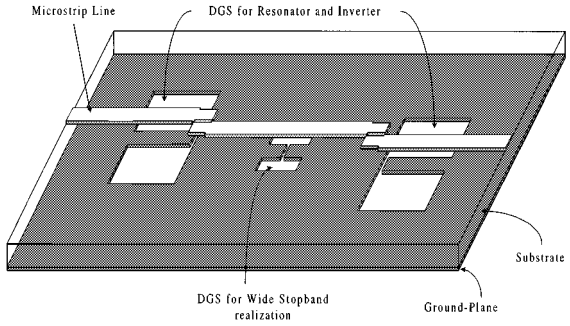


Fig. 12. Schematic of the DGS coupled-line filter with an additional DGS section in the coupled resonator.

three-pole bandpass filter at the center frequency of 4 GHz with an attenuation pole in the upper stopband, which is realized by the DGS. The bandwidth is 10% with a ripple level of 0.05 dB. The attenuation-pole location was also chosen to be 4.9 GHz, which corresponds to the self-resonant frequency of the DGS circuit. In order to realize the designed bandpass filter, the DGS circuit should implement the parallel *LC* resonator circuit shown in Fig. 8(a). Fig. 8(b) shows the proposed DGS configuration and designed dimension, which corresponds to the equivalent circuit shown in Fig. 8(a). By employing simulations on the equivalent circuit and DGS, we can verify the determined dimension of the DGS section. Comparison between the calculated $S$-parameter of the designed DGS section and simulated data for its equivalent circuit shows good agreement, as shown in Fig. 9. The $S$-parameter of the DGS section was calculated by HFSS v.7.0. Simulation on the equivalent circuit was done by Serenade v.8.0. We can see a

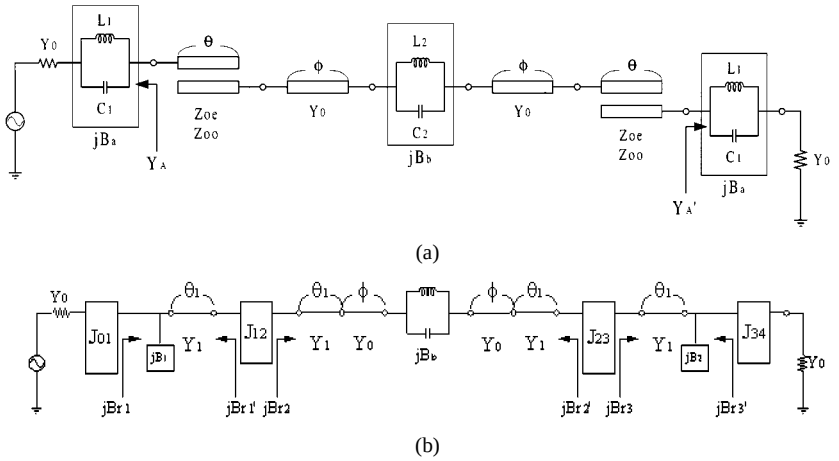


Fig. 13. (a) Circuit representation of the proposed DGS coupled-line bandpass filters with an additional DGS circuit. (b) Its equivalent circuit with $J$-inverters.

resonance frequency at 4.9 GHz, which exactly coincide with the attenuation-pole location of the design specification [8], [9].

The designed coupled-line bandpass filter was fabricated and then measured. The substrate for fabrication was chosen to be CER-10-TACONIC, which has a dielectric constant of ten of 62-mil thick. Fig. 10 shows the comparative results between simulation and measurement on the fabricated three-pole bandpass filter. Measurements agree relatively well with theoretical results, as shown in Fig. 10. Measured insertion and return losses are less than 1.0 and 25 dB, respectively. An attenuation-pole location appears at 4.9 GHz and the rejection level at this frequency shows approximately 35 dB. Fig. 11 presents a photograph of the fabricated DGS coupled-line filter, which has characteristics of a three-pole bandpass filter. Although a three-pole bandpass filter with a single mode needs three resonators, there is only a single coupled resonator with two DGS sections. The slightly higher insertion loss compared to the simulated data can be due to the finite unloaded $Q$ of the microstrip resonator and the radiation loss of the etched DGS sections. The insertion-loss characteristics can be improved by properly shielding the overall DGS coupled-line filter.

## IV. Improvement of Stopband Characteristic

We have demonstrated and proven that the proposed DGS coupled-line filter enables us to have a simple fabrication with compact size, improved stopband characteristic with an attenuation pole, and a relatively good insertion-loss characteristic. However, a concern of a more improved stopband characteristic with multiple poles of attenuation still remains. In this section, we extend our design method for a DGS coupled-line filter to the implementation of multiple attenuation poles, which can be obtained by adding additional DGS sections. Fig. 12 shows the schematic of a DGS coupled-line filter with an additional DGS section in the coupled resonator.

Fig. 13 shows the symmetrical coupled-line bandpass filter configuration with an additional DGS section and its equivalent circuit with $J$-inverters. In order to obtain the inverter formula, derivation of susceptance for each resonator needs to be preceded. The only difference between equivalent circuits, shown in Figs. 3 and 13, is that there is a parallel $LC$ circuit at the second resonator section due to the additional DGS. Thus, susceptances for the first and the third resonators of the equivalent circuit shown in Fig. 13 are identical to those of the equivalent circuit shown in Fig. 3. This means that we can directly use the $J$-inverter formulas of (13) and (16) for this equivalent circuit. However, the susceptance of the second resonator seen in Fig. 13 is given by

$$jB_{r2} = jY_1 \tan(\theta_1 + \phi') = jB'_{r2} \tag{17}$$

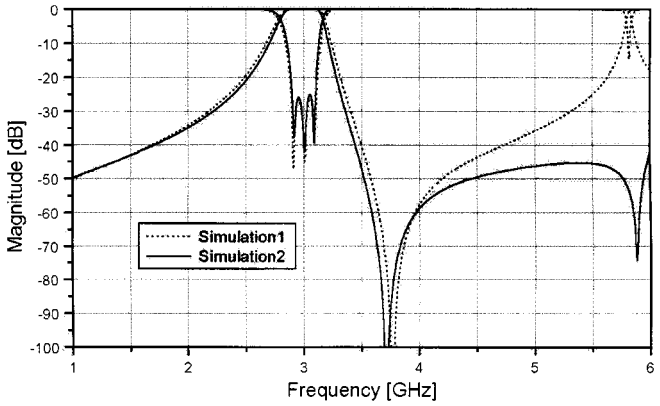


Fig. 14. Comparison results of the simulated $S$-parameters between the DGS coupled-line filters without an additional DGS section (Simulation 1) and with an additional one (Simulation 2).

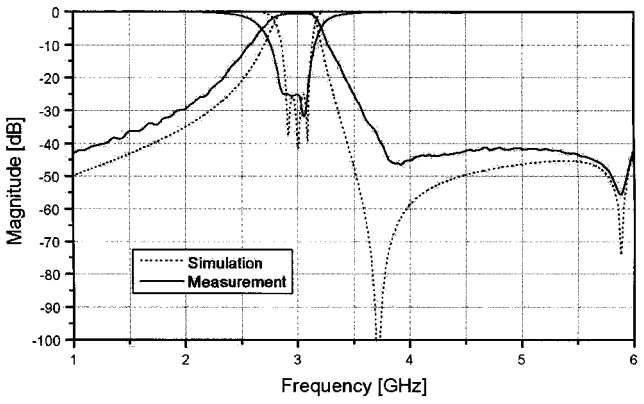


Fig. 15. Comparison results between simulation and measurement on the fabricated DGS coupled-line bandpass filter with an additional DGS section.

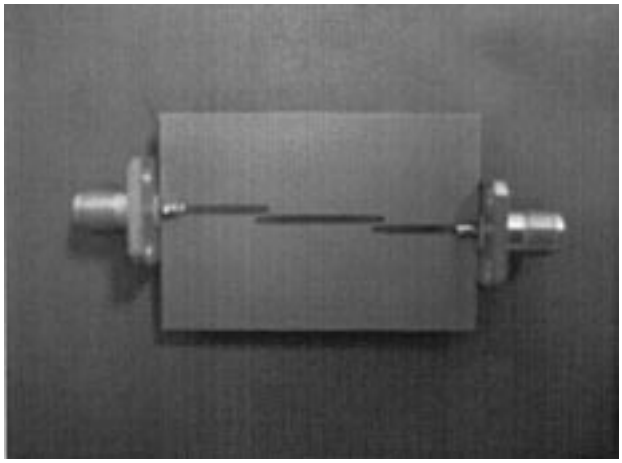

(a)

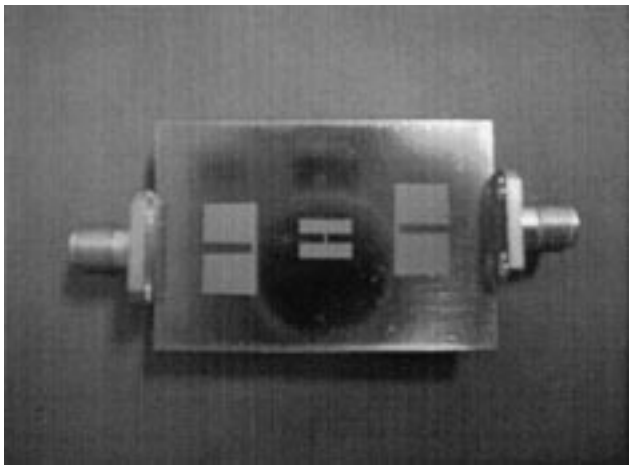

(b)

Fig. 16. Fabricated DGS coupled-line bandpass filter with an additional DGS. (a) Top view. (b) Bottom view.

where $\phi' = \tan^{-1}\{(Y_0/Y_1)\tan(\gamma+\phi)\}$, $\gamma = \tan^{-1}(B_e/Y_0)$, $jB_e = j(Y_0\tan(\phi+\beta))/(1+(Y_0/B_b)\tan(\phi+\beta))$, and $\beta = \tan^{-1}((Y_1/Y_o)\tan\theta_1)$.

If $Y_1$ equals $Y_o$, then the susceptance of the second resonator is given by

$$jB_{r2} = jY_0\left\{\frac{B_c + Y_0\tan(\theta_1+\phi)}{Y_0 - B_c\tan(\theta_1+\phi)}\right\} = jB'_{r2} \tag{18}$$

where $jB_c = j\{(B_bY_0\tan(\theta_1+\phi))/(B_b - Y_0\tan(\theta_1+\phi))\}$.

Thus, the $J$-inverter formulas of (14) and (15) should be modified by using the derived susceptance equations of (17) or (18). In addition, by using resonance conditions of the second resonator, electrical lengths for the coupled-line resonator section can be derived as follows:

$$\phi = \tan^{-1}\left(-\frac{2B_b}{Y_0}\right) - \theta_1. \tag{19}$$

To demonstrate the improved stopband performance of the proposed coupled-line bandpass filter with an additional DGS section, we designed a DGS bandpass filter at the center frequency of 3 GHz with two attenuation poles in the upper stopband. The basic specification was a 2.9–3.1-GHz passband with a 0.01-dB ripple level and rejection of 40 dB up to 6 GHz. Theattenuation-pole locations have been chosen to be 3.7 and 5.9 GHz. Fig. 14 shows comparative results of the simulated $S$-parameters between the DGS coupled-line filters with an additional DGS section and without an additional one. Since a DGS section has a self-resonant characteristic, this additional DGS section of the resonator can also provide an extra attenuation pole in the upper stopband. Due to this extra attenuation-pole location, the stopband performance can be significantly improved compared to that of the DGS coupled-line filter without an additional DGS section of a resonator, as shown in Fig. 14. Furthermore, rejection at the first attenuation-pole location shows deeper performance than that of the second one, as shown in the simulated data. This can be due to the overlapped resonant frequencies of the DGS sections at the in–out ports. The designed coupled-line bandpass filter was fabricated using a Duroid ($\epsilon_r = 10.2$) substrate. The thickness of the substrate is 1.27 mm. Fig. 15 shows measurements on the fabricated DGS coupled-line filter with an additional attenuation pole. As shown in Fig. 15, the spurious-free stopband is extended to 6 GHz with excellent insertion-loss performance. A photograph of the fabricated hardware is shown in Fig. 16. We can obtain more extended stopband performance by pushing the resonant frequency of an additional DGS section out of the interesting frequency band.

## V. Conclusion

A novel coupled-line bandpass filter with a DGS has been proposed and demonstrated in this paper. The equivalent circuit and the related design procedures have been discussed in detail. The design equations for the proposed coupled-line bandpass filter have been derived based on the coupled-line filter theory and the equivalent circuit of DGS. In order to show the validity of the proposed coupled-line bandpass filter structure and design method, an example of a three-pole bandpass filter has been achieved. The experimental results on a fabricated bandpass filter show excellent loss characteristics and attenuation-pole location at 4.9 GHz. Furthermore, the extended design approach of the proposed DGS coupled-line filter has also been presented. The approach has shown that by employing an additional DGS section, the stopband performance of the proposed DGS filter is significantly improved. The newly proposed DGS coupled-line filter and the related design method are readily compatible with monolithic microwave integrated circuit (MMIC) or multilayer technology and should find a wide range of applications.

## References

[1] T. J. Ellis and G. M. Rebeiz, "MM-wave tapered slot antennas on micromashined photonic bandgap dielectrics," in *IEEE MTT-S Int. Microwave Symp. Dig.*, June 1996, pp. 1157–1160.

[2] V. Radisic, Y. Qian, and T. Itoh, "Broad-band power amplifier using dielectric photonic bandgap structure," *IEEE Microwave Guided Wave Lett.*, vol. 8, pp. 13–14, Jan. 1998.

[3] M. P. Kesler, J. G. Maloney, and B. L. Shirley, "Antenna design with the use of photonic bandgap material as all dielectric planar reflectors," *Microwave Opt. Technol. Lett*, vol. 11, no. 4, pp. 169–174, Mar. 1996.

[4] V. Radisic, Y. Qian, R. Coccioli, and T. Itoh, "Novel 2-D photonic bandgap structure for microstrip lines," *IEEE Microwave Guided Wave Lett.*, vol. 8, pp. 69–71, Feb. 1998.

[5] C. S. Kim, J. S. Park, D. Ahn, and J. B. Lim, "A novel one-dimensional periodic defected ground structrure for planar circuits," *IEEE Microwave Guided Wave Lett.*, vol. 10, pp. 131–133, Apr. 2000.

[6] H. T. Kang, J. S. Yun, C. S. Kim, J. S. Park, D. Ahn, and G. Y. Kim, "A study on the implementation of slow-wave structure using photonic bandgap configuration," in *Proc. IEEE MTT/AP/EMC Korea Chapter Microwave Wave Propagat.*, vol. 22, May 1999, pp. 187–190.
[7] C. S. Kim, J. S. Park, D. Ahn, and G. Y. Kim, "A design of 3 dB power divider using slow-wave characteristic," *J. Korean Electromagn. Eng.*, vol. 3, no. 3, pp. 694–700, Sept. 1999.
[8] J. I. Park, C. S. Kim, J. S. Park, Y. Qian, D. Ahn, and T. Itoh, "Modeling of photonic bandgap and its application for the low-pass filter design," in *Asia–Pacific Microwave Conf. Dig.*, Dec. 1999, pp. 331–334.
[9] D. Ahn, J. S. Park, C. S. Kim, Y. Qian, and T. Itoh, "A design of the low-pass filter using the novel microstrip defected ground structure," *IEEE Trans. Microwave Theory Tech.*, vol. 49, pp. 86–93, Jan. 2001.

**Jun-Seok Park** (S'95–A'99) was born in Seoul, Korea, on August 12, 1969. He received the B.S. and M.S. degrees in electronic engineering and the Ph.D. degree in radio frequency and monolithic microwave and integrated circuits from Kookmin University, Seoul, Korea, in 1991, 1993, and 1996, respectively.

In 1997, he joined the Department of Electrical Engineering, University of California at Los Angeles, where he was a Post-Doctoral Researcher. In March 1998, he joined the Division of Information Technology Engineering, Soonchunhyang University, Asan, Korea, where he is currently an Assistant Professor and Director of the Super-Module Research Laboratories. He is also currently the Technical Advisor of several RF/microwave component and system companies such as Netel Inc, Amotech Corporation, and SMR-Tech Inc. His current research involves RF and microwave hybrid module design using low-temperature co-fired ceramic techniques and RF integrated circuit (RFIC) design such as a power amplifiers for mobile handsets based on CMOS technology. His group has developed several novel components with a DGS. His group has also worked extensively in the area of various RF and microwave components with a novel configuration and design method.

**Jun-Sik Yun** was born in Seoul, Korea, in 1973. He received the B.S. and M.S. degrees in electrical and electronic engineering from Soonchunhyang University, Asan, Korea, in 1999 and 2001, respectively.

He is currently an Application Engineer with Ansoft Corporations, Seoul, Korea. His recent research interests include modeling of novel DGSs and their application for microwave and millimeter wave.

**Dal Ahn** (M'93) was born in Kimje, Korea, on October 15, 1961. He received the B.S., M.S., and Ph.D. degrees from Sogang University, Seoul, Korea, in 1984, 1986 and 1990, respectively, all in electronics.

From 1990 to 1992, he was with the Mobile Communications Division, Electronics and Telecommunications Research Institute (ETRI), Daejeon, Korea. Since 1992, he has been with the School of Electrical and Electronic Engineering, Soonchunhyang University, Asan, Korea, where he is currently an Associate Professor. He is also currently Chief of the RF and Microwave Component Research Center (RAMREC), Soonchunhyang University. He is a technical consultant with Tel Wave Inc., Suwon, Korea. He is an editor of the *Journal of the Korean Electromagnetic Engineering Society*. His current research interests include the design and application of passive and active components at radio and microwave frequencies, design of the RF front-end module for various handset system using low-temperature co-fired ceramic (LTCC) technology, DGS circuit applications, and circuit modeling using commercial electromagnetic analysis program.